Saffil alumina fibers reinforced dual-phase Mg-Li and Mg-Li-Zn alloys

S. Kúdela Jr.[1]*, P. Švec[2], O. Bajana[1], Ľ. Orovčík[1], P. Ranachowski[3], Z. Ranachowski[3]

[1]*Institute of Materials & Machine Mechanics, Slovak Academy of Sciences,*
Dúbravská cesta 9, 845 13 Bratislava, Slovak Republic
[2]*Institute of Physics, Slovak Academy of Sciences, Dúbravská cesta 9, 845 11 Bratislava, Slovak Republic*
[3]*Institute of Fundamental Technological Research, Polish Academy of Sciences,*
Pawinskiego 5B, 02-106 Warszawa, Poland

Abstract

The gas pressure infiltration technique was used to prepare Saffil alumina fibers reinforced Mg-Li and Mg-Li-Zn matrix composites with a dual-phase matrix structure. There was investigated the effect of variable Li content (6.2–10.3 wt.% Li) and Zn alloying (~ 1.5 wt.% Zn) on the proof stress $R_p0.2$ of prepared composites. $R_p0.2$ values increased monotonously with rising fraction of Saffil fibers (5, 10 and 15 vol.%) reaching the maximum of about 250 MPa for Mg-Li matrix composites. $R_p0.2$ values of Mg-Li-Zn matrix composites were lower. Strengthening effect of Saffil fibers was promoted by the displacement redox reaction with Mg-Li and Mg-Li-Zn melts in which only Li significantly participated. Zn alloying retarded the displacement redox reaction. Too extensive reaction, however, resulted in the fiber damage and the drop in composite strength.

K e y   w o r d s: Mg-Li alloys, Saffil fibers, metal matrix composites, short-fiber strengthening, reactive wetting, displacement reactions

1. Introduction

Mg-Li alloys as the lightest known metallic structural materials (1.3–$1.6\,\mathrm{g\,cm^{-3}}$) offer great weight-saving potential for various structural applications. Their serious drawback is, however, poor strength level so that alloying with third element X (usually Al, Zn) is used to initiate the age hardening through the formation of transition $MgLi_2X$ phase. This strengthening effect is, nevertheless, unstable as the transformation to equilibrium LiX phase starts even at the room temperature resulting in the overaging [1]. Another strengthening possibility is the reinforcement of Mg-Li matrix with refractory fibers and/or particles wherein the short fiber reinforcement appears to be more promising alternative.

The pressure infiltration technique turned out to be a suitable method for the fabrication of short Saffil alumina fibers (SF) reinforced Mg-Li matrix composites [2]. The crucial problem of this process is, however,

the reactivity of Mg-Li melt against alumina phases. Both Mg and Li can participate in displacement redox decomposition of alumina producing MgO and Li_2O oxides and releasing elemental Al. Schematically:

$$(6/n)\mathrm{Me} + 2\mathrm{Al}^{3+} = (6/n)\mathrm{Me}^{n+} + 2\mathrm{Al}, \qquad (1)$$
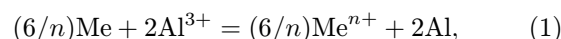
where Me is Mg or Li and n is valency. The Gibbs free energy data show that there are strong thermodynamic driving forces for the Eq. (1) at temperatures relevant for the melt infiltration process (50–$750\,^{\circ}\mathrm{C}$) [3]. As Li is principal reaction agent, its concentration governs the kinetics and extent of this displacement reaction. Equation (1) can facilitate the adhesion between SF and Mg-Li matrix (reactive wetting). Nevertheless, there is a great risk of the structural damage of SF.

The aim of the present work is to investigate the interaction of Mg-Li and Mg-Li-Zn alloys with SF during the melt infiltration process to elucidate the effect

*Corresponding author: tel.: +421 2 32401029; e-mail address: ummskudm@savba.sk

Table 1. Actual chemical composition of Mg-Li and Mg-Li-Zn alloys studied and fraction of α-phase [4]

Alloy	Composition (wt.%)	α-phase (vol.%)
A	Mg-6.24%Li	74.5
B	Mg-8.92%Li	33.2
C	Mg-9.98%Li	24.0
D	Mg-6.12%Li-1.42%Zn	78.9
E	Mg-8.64%Li-1.62%Zn	36.6
F	Mg-10.3%Li-1.63%Zn	18.4

of interfacial chemistry on the proof stress $R_{\rm p}0.2$ of prepared composites. The present paper is a continuation of our recent study dealing with the strengthening in dual-phase Mg-Li and Mg-Li-Zn alloys [4]. These alloys possess dual-phase $\alpha + \beta$ structure which combines the strength of h.c.p. α-phase with the ductility of b.c.c. β-phase [5]. The same Mg-Li and Mg-Li-Zn alloys have also been used as the matrices for the preparation of SF reinforced composites in the present work.

2. Experimental

2.1. Composite preparation

Six matrix alloys with nominal compositions of Mg-6Li (A), Mg-9Li (B), Mg-10Li (C), Mg-6Li-1.5Zn (D), Mg-9Li-1.5Zn (E) and Mg-10Li-1.5Zn (F) were prepared by the melting of pure magnesium, lithium and zinc metals (99.9, 99.0 and 99.9 %, respectively) in a mild-steel crucible under argon pressure of 0.5 MPa after previous evacuation. Actual alloys composition as determined by the atomic emission spectroscopy is presented in Table 1. According to Mg-Li phase diagram, these alloys should exhibit dual-phase $\alpha + \beta$ structure (5.5–11.2 wt.% Li) [6]. As the eutectic point is at 8 wt.% Li, the alloys A and D are hypo-eutectic ones while those B, C, E and F are hyper-eutectic.

The preforms of Saffil fibers (Saffil Ltd, UK) were infiltrated with above mentioned Mg-Li and Mg-Li-Zn alloys to fabricate the composite samples. The preform embedded in a steel holder consists of planar-randomly arranged Saffil fibers (5, 10 and 15 vol.%) without any binder. Individual fibers consist of nanocrystalline δ-Al$_2$O$_3$ phase with ~ 4 wt.% of dissolved SiO$_2$ and are typically 3–5 μm in diameter and about 600–1300 μm in length. Their tensile strength is declared as ~ 2000 MPa [7]. The melt infiltration was carried out by the vacuum-pressure technique in labor autoclave at 700 ℃ for 60 s under an argon pressure of 6 MPa.

2.2. SEM observations

The structure of composites studied was exam-

ined using the scanning electron microscope (SEM, Jeol JSM 7600F) equipped with Retractable Backscattered Electron Detector (RBEI). Before being SEM inspected and EDX analyzed, the specimens were metallographically polished to a mirror-like finish without etching. Energy dispersive spectrometer operating at 15 kV was used for elemental analysis.

2.3. XRD analysis

X-ray diffraction (XRD) records were acquired from metallographically polished sample surfaces using CuKα radiation using Bruker D8 diffractometer.

2.4. Microhardness measurements

Microhardness measurements were conducted on metallographically prepared alloy and composite surfaces using the FM-1E microhardness tester equipped with a Vickers indenter by imposing a load of 5 gf for 10 s. The microhardness data of each of α- and β-phases were taken from 20 randomly selected sites in both the matrix alloys and corresponding composites. The microhardness HV(5) values were determined as an arithmetic mean value of measured data.

2.5. Compression tests

Cylindric samples (ø 4 mm, length 8 mm) were prepared by turning operations from both naturally aged A–F alloys and corresponding A–F composites. The prepared samples were compression strained parallel to the fiber planes in ZWICK Z100 apparatus to determine the proof stress $R_{\rm p}0.2$ from engineering stress-strain curves.

3. Results

3.1. SEM observations

Figure 1 shows the series of SEM micrographs of the structure of 10 vol.% SF reinforced Mg-Li and Mg-Li-Zn matrix composites to demonstrate the effect of Zn alloying (~ 1.5 wt.%) and variable Li content (6.2–10.3 wt.%) on the microstructure. The micrographs of
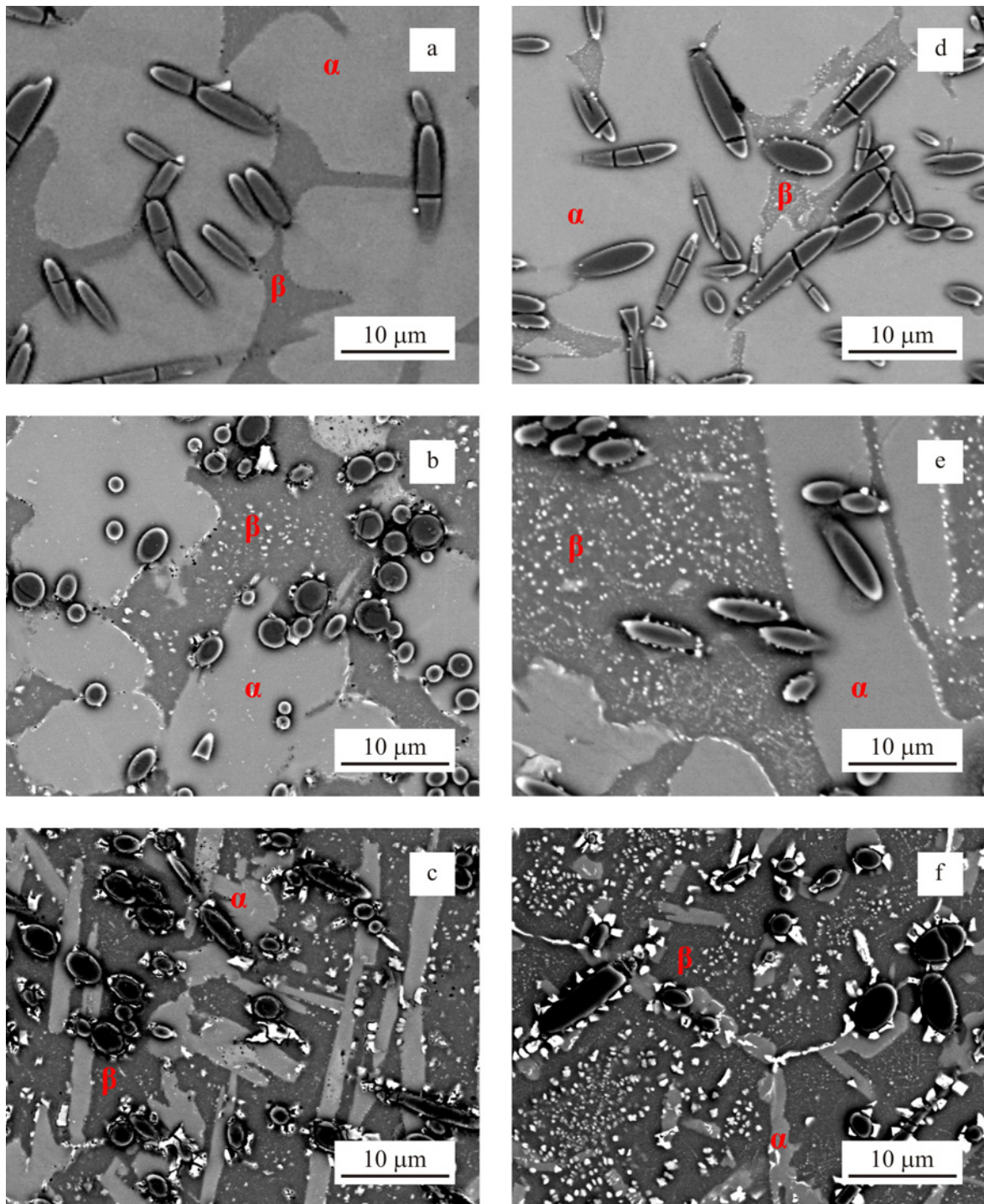
Fig. 1. SEM images (BSE mode) of the microstructure of 10 vol.% SF reinforced both Mg-Li matrix composites A–C (a)–(c) and Mg-Li-Zn matrix composites D–F (d)–(f) perpendicularly to the planar-random fibers array.

Mg-Li based composites A–C (Figs. 1a–c) and Mg--Li-Zn based ones D–F (Figs. 1d–f) are taken in BSE mode in which the darkness – brightness scale correlates with the atomic mass of alloying elements. Accordingly, the bright spots are indicative of Al and Zn distribution within the dual-phase $\alpha + \beta$ matrix structure. It is seen that increase in Li content decreases the fraction of α-phase and enriches the matrix regions with Al. Since Zn content remains constant the rising population of bright spots is clearly at the expense of Al release from SF.

In low Li alloyed composites A and D (6.2 and 6.1 wt.% Li) owing to negligible reaction extent no significant chemical damage of SF has occurred. Par-
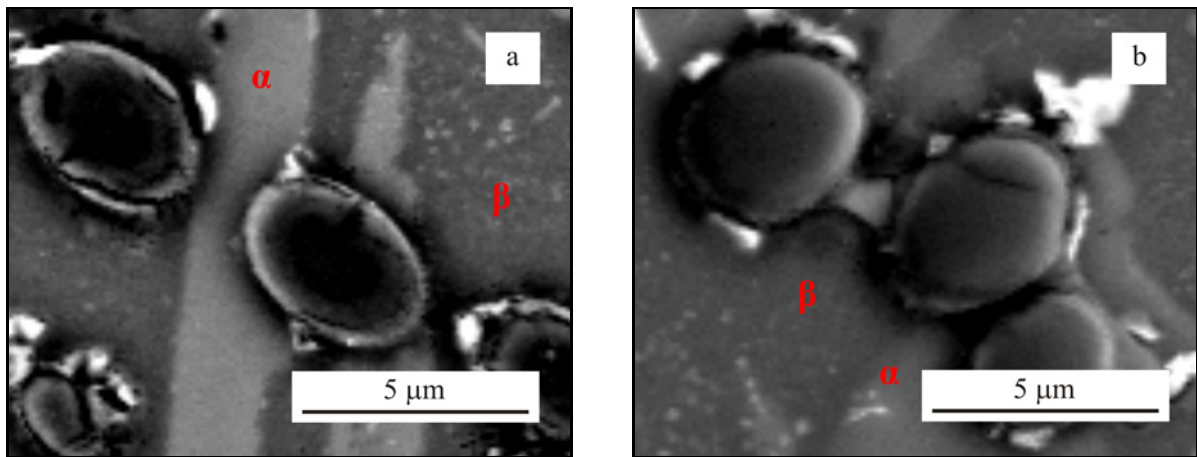
Fig. 2. SEM image of the details of the cross-section of Saffil fibers in composite C (a) and composite F (b) demonstrating retarding effect of Zn alloying on the fiber attack.
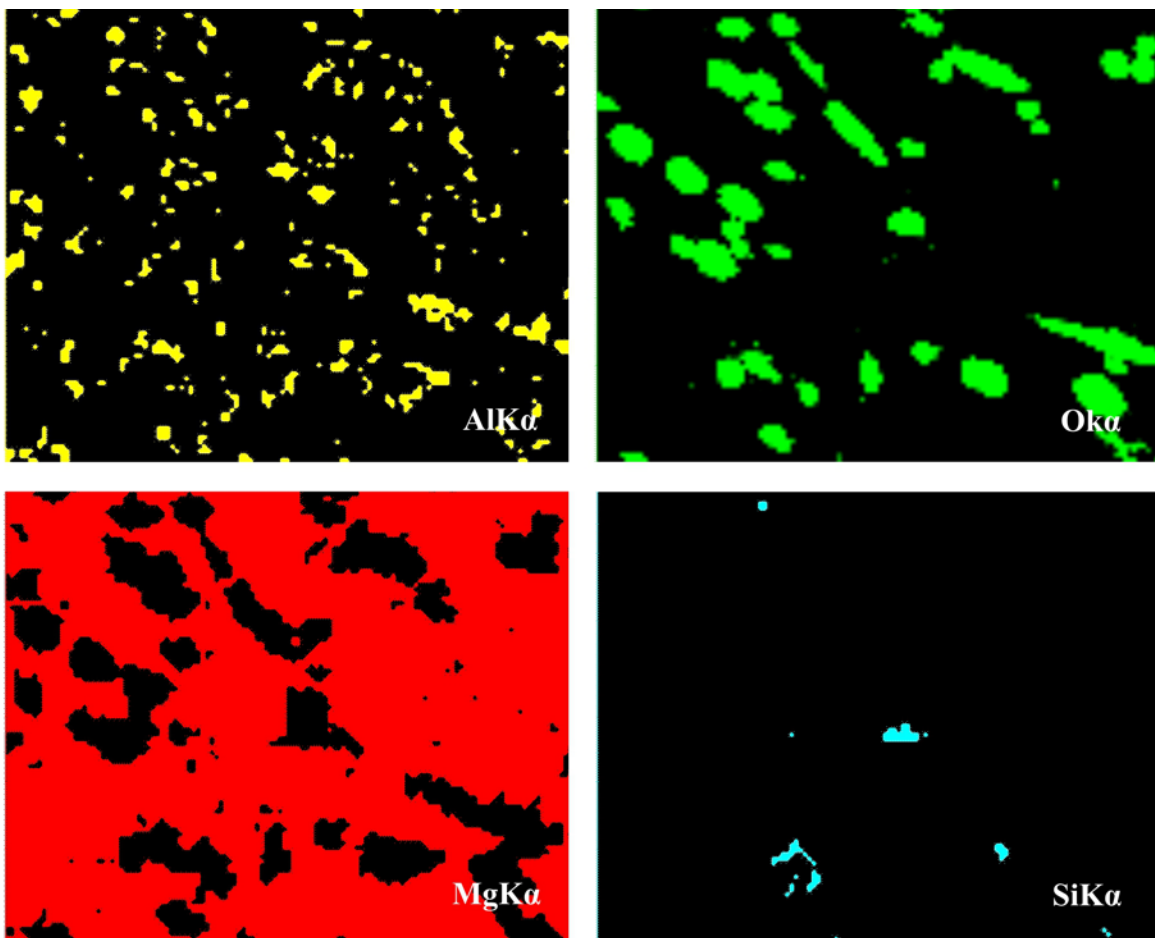
Fig. 3. Elemental EDX mapping of Al, Mg, O and Si in composite C (coupled with Fig. 1c).

ticularly no Al release is recognizable in Mg-Li based composite A (Fig. 1a). In Mg-Li-Zn based composite D the bright spots appear only in β-phase and should be attributed to Zn precipitating usually on SF surfaces (Fig. 1d).

In medium Li alloyed composites B and E (8.9 and

8.6 wt.% Li) higher Li content intensifies the chemical attack of SF. As a result, the fiber cross-section morphology in Mg-Li based composite B is partly modified, but the structural integrity of SF is still preserved (Fig. 1b). Neither morphological change nor chemical damage of SF can be observed in Mg-Li-Zn based com-
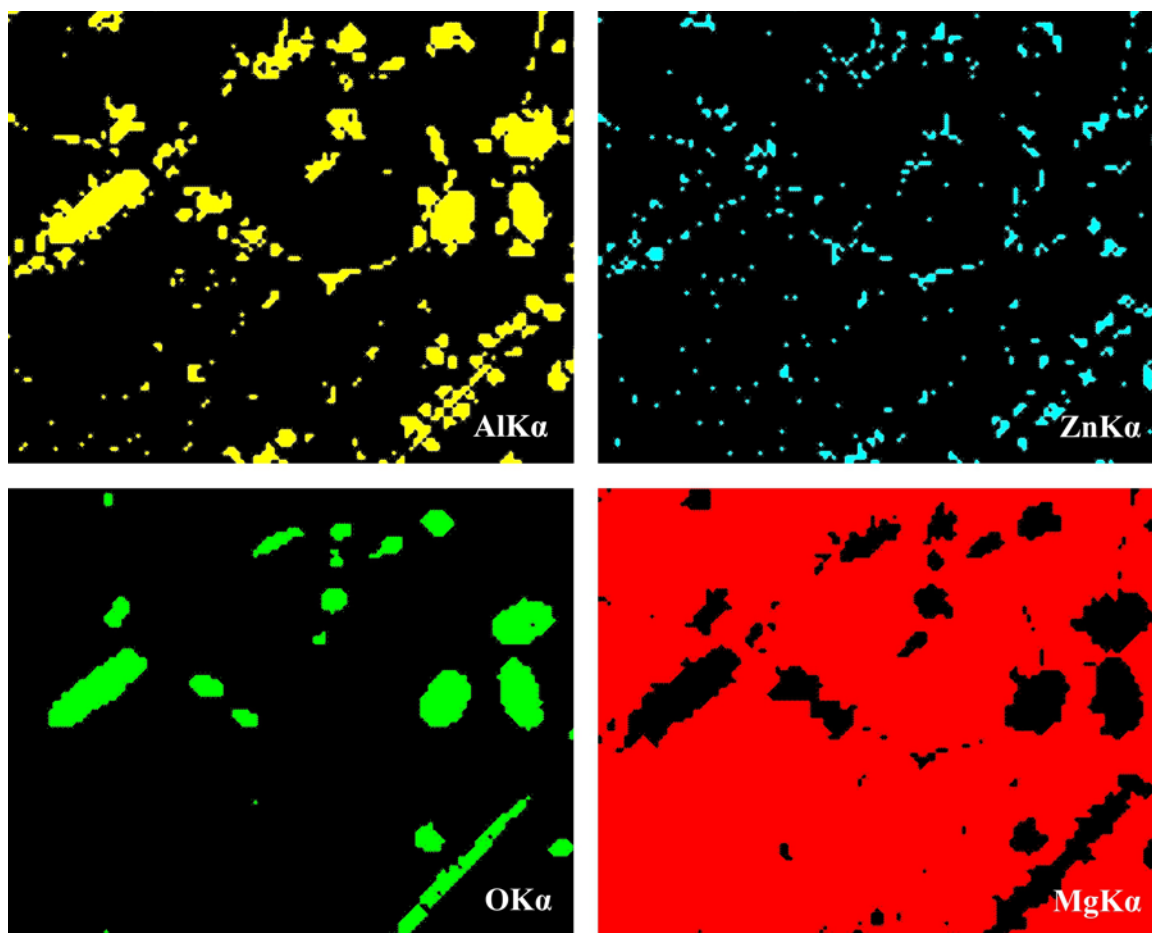
Fig. 4. EDX mapping of elements Al, Zn, Mg and O in composite F (coupled with Fig. 1f).

posite E (Fig. 1e). In both B and E composites, the released Al occurs preferentially in β-phase at α/β interfaces in particular while Zn tends to be accumulated on SF surfaces in composite E.

Extensive chemical attack of SF has occurred in highly Li alloyed composites C and F (9.98 and 10.3 wt.% Li). As a result, the cross-section morphology of SF in Mg-Li based composite C is largely modified exhibiting the signs of some structural fiber degradation (Fig. 1c). Moreover, coarse Al precipitates (2–3 μm in size) are distributed in β-phase. The decomposition of SF in composite F is evidenced by the dissemination of coarse Al precipitates over the β-phase and at the fiber surfaces in particular (Fig. 1f). Figure 2 compares the details of the cross-section structure of SF in composites C and F demonstrating that the fibers in sample C are largely destroyed while those in sample F appear to be almost unaffected.

3.2. EDX analysis

SEM micrographs of highly Li alloyed samples C and F have been completed with EDX mapping to characterize the chemical pathways of Mg, Al and Zn

elements during the reaction of SF with molten Mg--Li and Mg-Li-Zn matrix alloys. Note that Li cannot principally be detected by EDX technique.

EDX mapping of composite C (Fig. 3) is coupled with EBS image in Fig. 1c. It is seen that AlKα and OKα signals do not coincide thus suggesting that nearly total decomposition of SF has occurred. It is also seen that Al extracted from SF produces large irregular precipitates within the β-phase. The fibers do not generate any MgKα signal thus confirming insignificant role of Mg in redox decomposition of SF.

EDX inspection of composite F shows that reaction between SF and Mg-Li-Zn melt has been accomplished to much lesser degree compared to the composite C. EDX maps in Fig. 4 (coupled with EBS micrograph in Fig. 1f) indicate that only partial extraction of Al from SF has occurred wherein the precipitates (probably AlLi) have been formed in the region of β-phase contouring usually the alumina fibers. It is noteworthy that Zn and Al distributions nearly coincide which might be indicative of their co-precipitation. Like the previous case, MgKα map shows that no significant reaction of Mg with SF has proceeded in composite F.

BSE images suggest that Al released during the

T a b l e 2. Microhardness HV5 values of α- and β-phase in initial Mg-Li and Mg-Li-Zn alloys and related 10 vol.% SF reinforced composites

| Sample | HV5 (MPa) | | | |
| | Alloy | | Composite (10 vol.% SF) | |
	α	β	α	β
A	56.1	52.1	65.2	71.1
B	55.6	54.7	80.0	77.0
C	56.1	53.8	105.3	83.2
D	58.9	63.5	64.8	67.7
E	64.1	62.4	70.2	69.3
F	68.3	64.2	85.6	78.7

redox decomposition of SF is located prevailingly in β-phase. Nevertheless, quantitative EDX analysis has confirmed that α-phase is more enriched with Al than β-phase. Accordingly, in hyper-eutectic Mg-Li and Mg-Li-Zn matrices (composites B, C, E and F) the Al content in α-phase has been found 1.4–2.3 times higher compared to that in β-phase. On the other hand, the hypo-eutectic matrices (composites A and D) show an opposite trend exhibiting higher Al content in β-phase. There has also been observed that Mg-Li-Zn matrices (composites D–F) are significantly less Al-enriched than binary Mg-Li ones (composites A–C).

3.3. XRD analysis

XRD analysis has been used to identify Al precipitates formed in the matrix region. The composites have been long-term stored at the room temperature so that new phases could be formed by the natural aging. There are shown XRD spectra acquired from 10 vol.% SF reinforced medium Li alloyed Mg-Li and Mg-Li-Zn alloys (composites B and E, respectively). The spectra show the angle segment roughly between 20° and 40° comprising the peaks of relevant Al and Zn intermetallic (Fig. 5).

XRD spectrum taken from the composite B contains besides major patterns of α- and β-phases also the peaks of stable AlLi phase and the traces of metastable $MgLi_2Al$ phase. On the other hand, in XRD record of composite E there occur the peaks of stable MgLiZn phase and also partly overlapped patterns of metastable $MgLi_2Zn$ and $MgLi_2Al$ phases. Phases Mg_7Zn_3 and $MgLi_2Zn$ detected in composite E have also been identified in unreinforced alloy E. It is nevertheless noteworthy that stable MgLiZn phase that has been detected in composite E absents in unreinforced alloy E despite roughly the same Zn and Li contents. This suggests that SF in composite E are favorable substrates for the nucleation of MgLiZn phase.
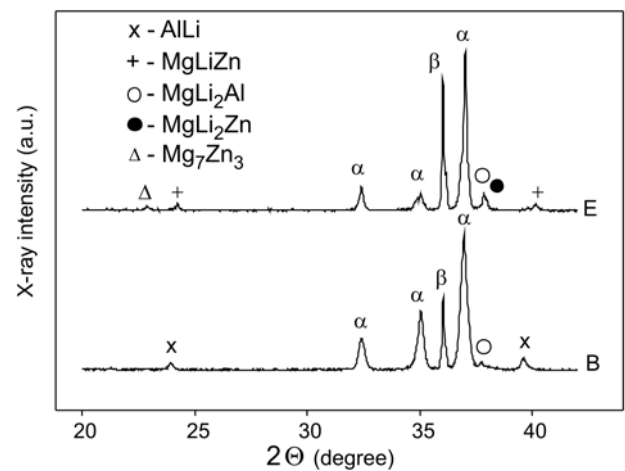
Fig. 5. XRD records taken from composites B and E in the segment of diffraction angles of 20°–40° comprising the patterns of relevant Al and Zn intermetallics.

3.4. Microhardness measurements

Dissolving of released Al in Mg-Li and Mg-Li-Zn matrices results in their hardening so that the microhardness data reflect the degree of redox decomposition of SF. Moreover, the microhardness measurements allow to recognize the Al distribution between α- and β-phases. Unlike the EDX and SEM observations, the microhardness data can monitor the effect of Li alloying on the decomposition reaction more precisely. The microhardness HV(5) data of α- and β-phases in Mg-Li and Mg-Li-Zn alloys and their 10 vol.% SF reinforced composites are presented in Table 2.

The microhardness values of α- and β-phases in Mg-Li alloys (A–C) indicate that α-phase is slightly stronger than β-phase. In Mg-Li-Zn alloys (D–F) the Zn alloying results in significant hardening of both α- and β-phases that however differ in their hardening responses: the microhardness of α-phase rises grad-
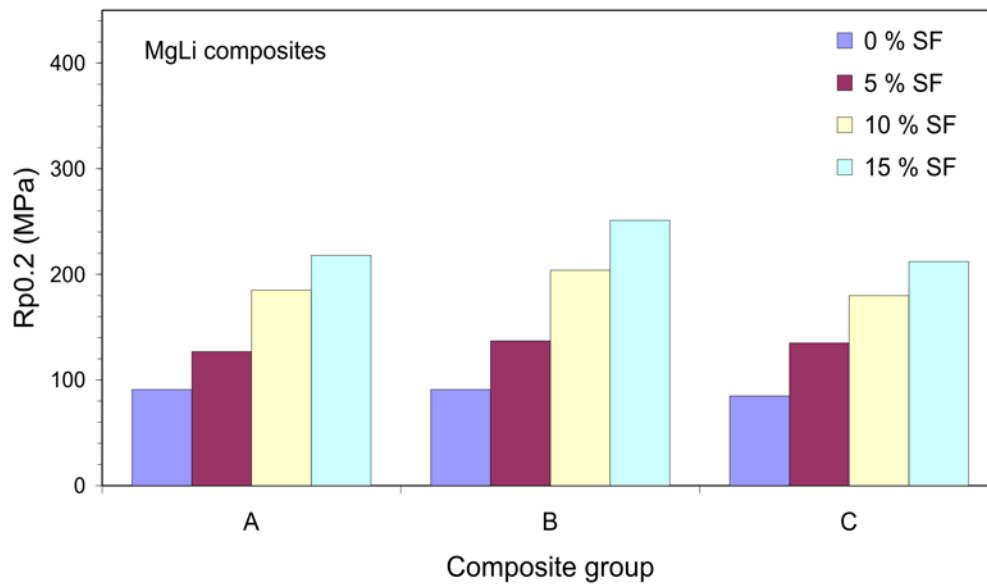
Fig. 6. Proof stress $R_{\mathrm{p}}0.2$ of Mg-Li based composites A, B and C containing different fractions of Saffil fibers (0, 5, 10 and 15 vol.%).

ually with increase in Li alloying while β-phase has been hardened suddenly exhibiting quite little HV(5) variations.

The microhardness values of α- and β-phases in Mg-Li and Mg-Li-Zn composites are much higher than those observed in unreinforced matrix alloys apparently due to the hardening with released Al. It is also seen that the matrix hardening in Mg-Li based composites (A–C) is considerably greater than that in Mg-Li-Zn based ones (D–F) thus underlining retarding effect of Zn alloying on the redox decomposition of SF.

An interesting observation is that in low Li alloyed matrices (composites A and D) greater hardening occurs in β-phase while in highly Li alloyed matrices (composites C and F) greater hardening occurs in α-phase. Generally, the released Al initiates greater hardening in a minority phase which corresponds with above reported Al enrichment of α- and β-phases in hyper- and hypo-eutectic Mg-Li and Mg-Li-Zn matrices (Sec. 3.2).

3.5. Compression tests

Cylindric composite samples have been compression strained parallel to the planar random fibers orientation to determine $R_{\mathrm{p}}0.2$ values from engineering stress-strain curves as a strengthening criterion. The $R_{\mathrm{p}}0.2$ data obtained have been evaluated with respect to the fraction of alumina fibers (0, 5, 10 and 15 vol.%) and the composition of matrix alloys (Li and Zn alloying). The $R_{\mathrm{p}}0.2$ values of Mg-Li and Mg-Li-Zn based composites are presented as the histograms in Figs. 6 and 7 respectively.

$R_{\mathrm{p}}0.2$ values of unreinforced Mg-Li alloys vary between 92 and 85 MPa exhibiting slight softening tendency with increase in Li content. The addition of ~ 1.5 wt.% Zn initiates solid solution hardening thus increasing $R_{\mathrm{p}}0.2$ values up to 105 MPa for medium Li alloyed Mg-Li-Zn alloy. Reinforcement of these alloys with SF increases rapidly their strength wherein $R_{\mathrm{p}}0.2$ values rise monotonously with growing SF fraction reaching the maxima of 251 MPa and 238 MPa for respective Mg-Li and Mg-Li-Zn based composites. $R_{\mathrm{p}}0.2$ values of these composites are largely influenced with Li alloying of matrices; this effect is nevertheless ambiguous.

As for Mg-Li based composites, the favorable effect of Li alloying on $R_{\mathrm{p}}0.2$ can be observed only for composites with low and medium Li alloyed matrices (composites A and B) in which $R_{\mathrm{p}}0.2$ values up to 251 MPa have been reached. On the other hand, the composite with highly Li alloyed matrix (composite C) exhibit inferior $R_{\mathrm{p}}0.2$ values apparently due to the damage of alumina fibers.

Different strengthening behavior exhibit Mg-Li-Zn based composites in which the fiber-matrix has been presumably retarded by Zn alloying. Accordingly, low and medium Li alloyed Mg-Li-Zn composites D and E show significantly lower $R_{\mathrm{p}}0.2$ values than corresponding Mg-Li composites A and B. Retarding effect of Zn alloying is more apparent in highly Li alloyed Mg-Li-Zn composite F in which no fiber destruction has occurred in contrast to highly Li alloyed Mg-Li composite C. Conclusively, the displacement redox reaction appears to promote the strengthening effect in present composites until the reaction extent is below
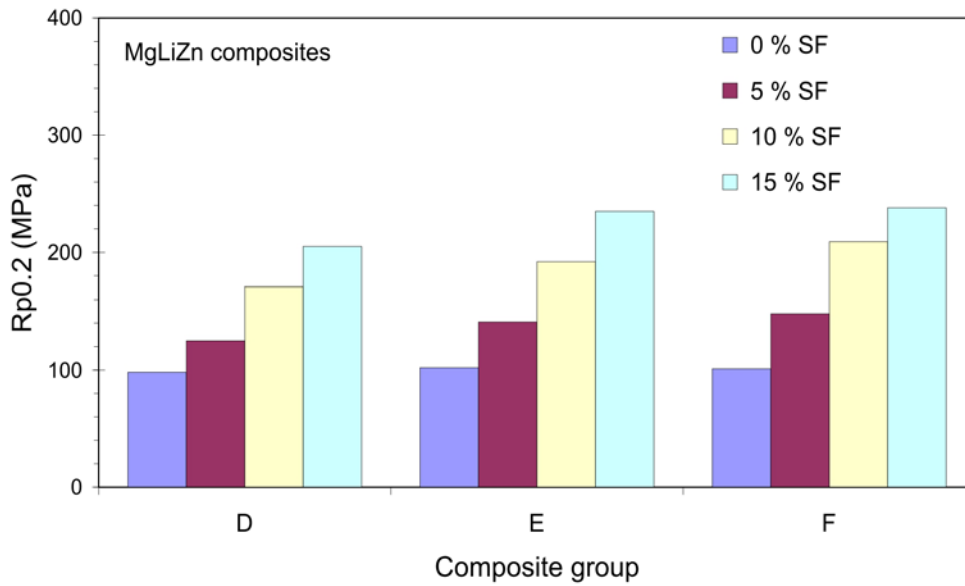
Fig. 7. $R_p0.2$ values of Mg-Li-Zn based composites D, E and F reinforced with different fractions of Saffil fibers (0, 5, 10 and 15 vol.%).

the critical value at which the fiber destruction starts to dominate.

4. Discussion

As shown above, during the infiltration of SF preform with Mg-Li and Mg-Li-Zn melts the redox decomposition of SF takes place producing elemental Al. There has also been concluded that Li is practically the only reaction agent while the role of Mg is marginal. Thermodynamic data, however, favor Mg possessing with greater thermodynamic potential than Li for displacement redox reaction with alumina [3]:

$$1/3Al_2O_3 + [Mg] = MgO + 2/3[Al],$$
$$\Delta G^\circ_{1000K} = -44.1 \, \text{kJ mol}^{-1} \, \text{MgO}, \qquad (2)$$

$$1/3Al_2O_3 + 2[Li] = Li_2O + 2/3[Al],$$
$$\Delta G^\circ_{1000K} = -17.7 \text{kJ mol}^{-1} \text{Li}_2\text{O}. \qquad (3)$$
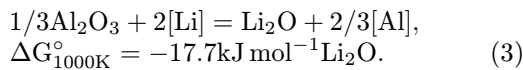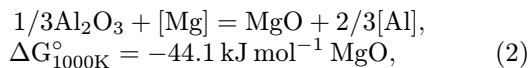
Experimentally observed higher reactivity of Li against SF is probably due to much higher diffusional mobility of Li compared to Mg. Another possible reason might be the surface activity of Li causing its enhanced concentration at the fiber surface.

The extent of SF decomposition can be estimated by the quantity of released Al using the stoichiometry of reaction (3). Accordingly, mean Al content in the matrix region of composite B containing 10 vol.% SF has been estimated by EDX as ∼ 2.7 wt.% Al that corresponds to the fibers decomposition degree of ∼ 21 %. This quite large value is indicative of the bulk nature of the fiber attack. It is thought that on the contact of SF with Mg-Li melt Li penetrates inside

the fibers by Knudsen's diffusion through the network of meso/micro-pores producing a Li_2O layer on pore walls by Eq. (3). Highly ionic Li_2O formed by Eq. (3) enters immediately the solid state reaction with adjacent δ-Al_2O_3 producing the non-stoichiometric Li--doped alumina phase assigned δ(Li). According to proposed reaction scheme, Li^+ ions occupy cationic vacancies in tetragonal δ-Al_2O_3 lattice transforming it to spinel-like δ(Li) phase while O^{2-} ions are joined to f.c.c. array of oxygen anions in δ-Al_2O_3 structure to keep the electrical neutrality [8]. Thus, the reaction of SF with molten Mg-Li alloys is rather complex process that can be schematically depicted as a sequence of following steps:

$$Al^{3+} + 3Li \rightarrow 3Li^+ + Al, \qquad (4)$$

$$Li + \delta\text{-}Al_2O_3 \rightarrow \delta(Li), \qquad (5)$$

$$Al \rightarrow [Al]_{\text{sol}}, \qquad (6)$$
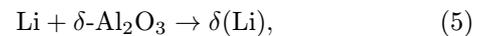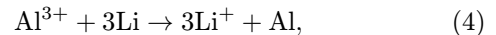
in which the solid-state reaction Eq. (5) is considered essential in terms of the formation of interfacial bond [2]. Nevertheless, the displacement reaction (Eq. (4)) is a kinetics governing step wherein elemental Al is dissolved in Mg-Li melt according to the Eq. (6). The δ(Li) product is crystallographically coherent with parental δ-Al_2O_3 phase so that no sharp boundary exists between them (topotaxy) [9]. As a result, despite quite large reaction extent, no dramatic structural changes of SF can occur in low and medium Li alloyed composites A, B, D and E. This is also the case of composite F in which the Eq. (4) is effectively retarded by Zn alloying. In more advanced reaction stage metastable δ(Li) product is transformed to

stable aluminates ($LiAl_5O_8$, $LiAlO_2$) that are structurally incoherent with δ-Al_2O_3 phase [10]. The appearance of new incoherent phase results in the loss of structural integrity of SF leading to their decay as demonstrated by the composite C.

Insertion of short alumina fibers into Mg-Li and Mg-Li-Zn matrices results in a rapid $R_p0.2$ increase. With some simplification, overall composite strengthening can be considered as the sum of the matrix hardening and the short-fiber strengthening based on the load transfer between the fibers and the matrix. Rapid increase in HV(5) with rising Li content shows that the matrix hardening is mainly attributable to released Al (Table 2). Considerable matrix hardening has occurred particularly in Mg-Li based composites (A–C) while that in Mg-Li-Zn based composites (D–F) is much lower due to retardation of Al release by Zn alloying. Retarding effect of Zn alloying on SF decomposition is rather surprising observation and is hardly chemically explainable as Zn is inactive against SF. At this point, one can only speculate about the adsorption of Zn on the surface of SF thus obstructing the Li access. Anyway, this phenomenon needs further study.

Apart from composites C in which massive destruction of SF has occurred, increase in matrix hardening HV(5) correlates with the rise in $R_p0.2$ values exhibiting clear dependence on Li alloying. Maximum $R_p0.2$ values (up to 251 MPa) have been reached for 15 vol.% SF reinforced Mg-Li based composite B. There is, however, a question how the matrix hardening contributes to overall $R_p0.2$ values of the composite. For instance, there has been determined $R_p0.2$ of 204 MPa for 10 vol.% SF reinforced composite B containing ~ 2.7 wt.% Al in the matrix region. For cast Mg-Li-Al alloy of similar composition (Mg-8 wt.% Li-3 wt.% Al) there was reported the tensile strength R_m of 142 MPa so that its $R_p0.2$ should be well below this value [11]. Therefore, the matrix hardening due to released Al appears to be too little, and high $R_p0.2$ values of present composites are mainly due to the short-fiber strengthening.

5. Conclusions

Saffil alumina fibers reinforced dual-phase Mg-Li and Mg-Li-Zn matrix composites were fabricated by the gas pressure infiltration technique. There was investigated the effect of variable Li content (6.2–10.3 wt.% Li) and Zn alloying (~ 1.5 wt.% Zn) in Mg-Li and Mg-Li-Zn matrices on the proof stress $R_p0.2$ of prepared composites. The results obtained are as follows:

– The displacement redox reaction between Saffil alumina fibers and molten matrix alloys took place on the pressure infiltration process in which Li was the only significant reaction agent. The displacement redox reaction was found to be retarded by Zn alloying.

– $R_p0.2$ values of prepared composites increased monotonously with rising fraction of Saffil fibers (5, 10 and 15 vol.%) and were higher for Mg-Li matrix composites reaching the maximum of about 250 MPa. Mg-Li-Zn matrix composites showed lower $R_p0.2$ values.

– Strengthening effect of Saffil fibers was promoted by the displacement reaction due to the reactive wetting. Therefore, $R_p0.2$ values of composites rose with an increase in Li alloying. Too extensive displacement reaction, however, resulted in the fibers damage and the drop in $R_p0.2$.

References

[1] Jackson, J. H., Frost, P. D., Loonam, A. C., Eastwood, L. W., Lorig, C. H.: Transactions AIMME, *185*, 1949, p. 149.
[2] Trojanová, Z., Drozd, Z., Kúdela, S., Száraz, Z., Lukáč, P.: Composites Science and Technology, *67*, 2007, p. 1965. doi:10.1016/j.compscitech.2006.10.007
[3] JANAF Thermochemical Tables. 2nd Edition. NSRDS/NBS 37. Washington, D.C., US Department of Commerce 1971.
[4] Kúdela Jr., S., Švec, P., Bajana, O., Orovčík, Ľ., Ranachowski, P., Ranachowski, Z.: Kovove Mater., *54*, 2016, p. 483. doi:10.4149/km2016_6_483
[5] Haferkamp, H., Jaschik, C., Juchmann, P., Kaese, V., Niemeyer, M., Tai, P.: Materialswissenschaft und Werkstofftechnik, *32*, 2001, p. 25. doi:10.1002/1521-4052(200101)32:1<25::AID-MAWE25>3.0.CO;2-J
[6] Nayeb-Hashemi, A. A., Clark, J. B., Pelton, A. B.: Bulletin of Alloy Phase Diagrams, *5*, 1984, p. 365. doi:10.1007/BF02872951
[7] Saffil® Technical Data Sheet, 2006.
[8] Kúdela, S., Oswald, S., Kúdela Jr., S., Baunack, S., Wetzig, K.: Journal of Alloys and Compounds, *378*, 2004, p. 127. doi:10.1016/j.jallcom.2003.10.090
[9] Kúdela, S., Rennekamp, R., Baunack, S., Gergely, V., Oswald, S., Wetzig, K.: Microchimica Acta, *127*, 1997, p. 243. doi:10.1007/BF01242730
[10] Kúdela, S., Gergely, V., Smrčok, Ľ., Oswald, S., Baunack, S., Wetzig, K.: Journal of Materials Science, *31*, 1996, p. 1595. doi:10.1007/BF00357869
[11] Wu, R., Qu, Z., Zhang, M.: Materials Science and Engineering A, *516*, 2009, p. 96. doi:10.1016/j.msea.2009.04.025